OPEN

NPG Asia Materials (2018) 10, e471; doi:10.1038/am.2017.224
www.nature.com/am

ORIGINAL ARTICLE

Bio-inspired superhydrophilic coatings with high anti-adhesion against mineral scales

Tianzhan Zhang[1,2], Yuefeng Wang[1,3], Feilong Zhang[3,4], Xiaodong Chen[3,5], Guoqing Hu[3,5], Jingxin Meng[1] and Shutao Wang[1,3]

The unexpected adhesion of certain inorganic minerals on solid surfaces is constantly a source of severe problems in daily life and industrial production, including scales in water pipes. Inspired by the nanostructured inner surface of normal renal tubules, we design a superhydrophilic nanohair coating composed of a poly(hydroxyethyl methacrylate) (PHEMA) hydrogel, which shows high anti-adhesion against mineral scales under flow conditions. Even at a high temperature of 80° C, the nanohair hydrogel coatings still show excellent anti-scaling performance compared to a flat hydrogel coating and a commercial water pipe with a polyvinylchloride (PVC) surface. The anti-scaling experiments and theory simulation reveal the crucial role of superhydrophilicity and fluid-assisted motion of the nanohairs in the anti-adhesion property. This study may provide promising insight into the design of high anti-adhesion coatings for resisting mineral scale attachment in water management systems.
NPG Asia Materials (2018) **10,** e471; doi:10.1038/am.2017.224; published online 9 March 2018

INTRODUCTION

Various unique surface adhesion phenomena have inspired considerable innovation and have served as the foundation to design novel adhesive materials based on biological systems,[1–3] such as geckos,[4–6] mussels,[7] sandcastle worms[8] and their combinations.[9] For example, gecko feet facilitate the development of skin adhesives/patches for biomedical materials[10] and flexible wearable devices.[11–15] Utilizing the bio-adhesion principle, the effective attachment of crystals has been studied, which is necessary for bone formation as well as teeth minerals.[16] In contrast, some unexpected surface adhesion (for example, mineral scales) often produce adverse influences on our daily lives and industrial production. For instance, mineral microcrystals tend to adhere onto the internal surface of pipelines used in heat exchangers and water-cooling towers and to further aggregate into stable mineral scales, thereby reducing work efficiency and even triggering equipment damage.[17,18] To alleviate these severe problems, much attention has been paid to the development of scale inhibitors[19,20] and water pretreatment systems.[21–23] However, these two strategies often cause water pollution and increased costs.[24] Recently, some attempts based on superwettability regulation[25–28], such as superhydrophobic copper oxide coatings with nanowires or nanoflakes, have been employed to prevent the growth and adhesion of mineral crystals.[29,30] However, the superhydrophobicity of surfaces may be gradually lost after immersion in a fluid for a long time, which probably hinders further applications of such system.[31] Therefore, it remains a great challenge to develop functional coatings with high anti-adhesion against mineral scales.

Kidney stones, one of the common calculous diseases, mainly originate from undesired adhesion and aggregation of mineral crystals onto the flattened surface of injured renal tubules.[32,33] Calcium oxalate crystals (CaOx), the primary inorganic constituent of kidney stones, hardly adhere onto the surface of normal renal tubules with nanohair structure[34,35] (Figure 1a), while injured tubules without nanohair practically lose this unique anti-stone capability (Figure 1b).[36–39] Moreover, there are many nanohairs on the surface of normal renal tubules. The hydrophilic domain of lipids and proteins in the nanohair-like membrane faces outward.[40,41] Thus, this unique anti-adhesive phenomenon from the inner surface of normal renal tubule greatly encourages us to design anti-scale coatings by mimicking the nanohair-like structure and hydrophilic properties of normal renal tubules.

Herein, inspired by the nanohair-like inner surface of normal renal tubule, we report that superhydrophilic nanohair coatings composed of a poly(hydroxyethyl methacrylate) (PHEMA) hydrogel exhibit high anti-adhesion against mineral crystals under flow conditions. Unlike the high mineral adhesion of flat hydrogel coatings shown in Figure 1d, nanohair hydrogel coatings exhibit high anti-adhesion against mineral crystals (Figure 1c). The anti-scaling experiments and theory simulation reveal the crucial role of superhydrophilicity and fluid-assisted motion of the nanohair in the anti-adhesion property.

[1]CAS Key Laboratory of Bio-inspired Materials and Interfacial Science, CAS Center for Excellence in Nanoscience, Technical Institute of Physics and Chemistry, Chinese Academy of Sciences, Beijing, China; [2]College of Material Science and Engineering, Jilin Jianzhu University, Changchun, China; [3]University of Chinese Academy of Sciences, Beijing, 100049, China; [4]Beijing National Laboratory for Molecular Sciences (BNLMS), Key Laboratory of Green Printing, Institute of Chemistry, Chinese Academy of Sciences, Beijing, China and [5]The State Key Laboratory of Nonlinear Mechanics, Institute of Mechanics, Chinese Academy of Sciences, Beijing, China
Correspondence: Professor J Meng or Professor S Wang, CAS Key Laboratory of Bio-Inspired Materials and Interfacial Science, Technical Institute of Physics and Chemistry, Chinese Academy of Sciences, 29 Zhongguancun East Road, Haidian District, Beijing, 100190, China.
E-mail: mengjx628@mail.ipc.ac.cn or stwang@mail.ipc.ac.cn
Received 15 July 2017; revised 18 October 2017; accepted 25 October 2017

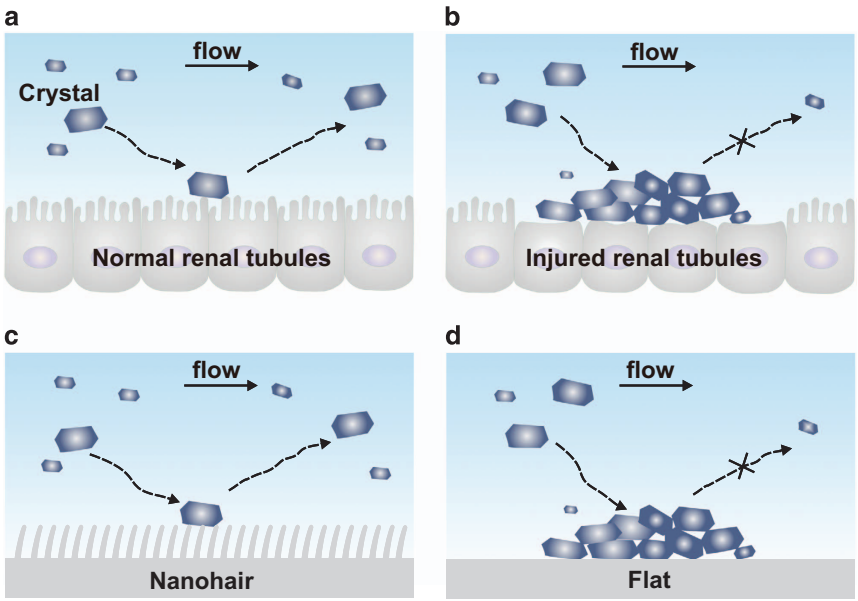

Figure 1 Schematic illustration of anti-adhesion performance against mineral crystals on renal tubules and the corresponding bio-inspired hydrogel coatings. In a flowing mineral solution, mineral crystals tend to detach from normal renal tubules with nanohairs (**a**) but adhere onto injured ones without nanohairs (**b**). For the corresponding bio-inspired hydrogel coatings, mineral crystals easily wash away from nanohair hydrogel coatings (**c**) but adhere onto flat hydrogel coatings (**d**).

Furthermore, under some harsh conditions when chemical inhibitors cannot work, such as high temperature, nanohair hydrogel coatings can retain their high anti-adhesion property, indicating their favorable mechanical stability. Therefore, this study will open up a new avenue to develop high anti-scaling materials for potential applications in various fields, such as water management systems.

EXPERIMENTAL PROCEDURES

Materials

Hydroxyethyl methacrylate (HEMA, 99%), ethylene glycol dimethacrylate (EGDMA, 99%), photoinitiator (Darocur 1173), sodium chloride (NaCl, 99%), sodium acetate trihydrate ($NaCOOCH_3$, 98%), sodium hydroxide (NaOH, 98%), calcium chloride ($CaCl_2$, 98%), sodium oxalate ($Na_2C_2O_4$, 98%), and sodium bicarbonate ($NaHCO_3$, 98%) were purchased from J&K Scientific, Beijing, China. All aqueous solutions were prepared using ultra-pure water (Milli-Q, Millipore, S.A.S., Molsheim, France). Anodic aluminum oxide (AAO) membranes with different depths (that is, 2, 40 and 60 μm) were purchased from Pu-Yuan Nanotechnology Limited Company, Hefei, China. All the reagents were used without further purification. Commercial water pipes with polyvinylchloride (PVC) surfaces were purchased from L&S Company, Beijing, China.

Procedures

Fabrication of Bio-inspired superhydrophilic surfaces. In our experiment, we prepared bio-inspired hydrogel coatings by integrating photopolymerization with a replica molding method.[42] First, a mixture of 3 ml of HEMA, 4 ml of H_2O and 75 μl of Darocur 1173 was stirred for 2 min and exposed to a mercury lamp (PLS-LAM500) for 4 min, obtaining a partially polymerized solution. Next, 50 μl of Darocur 1173 and 25 μl of EGDMA were added to the partially polymerized solution and then stirred for 2 min, obtaining a mixture of PHEMA precursor solution. Later, the PHEMA precursor solution was covered with an AAO template and illuminated under the mercury lamp for 1 h, leading to the formation of cured PHEMA. Finally, the nanohair hydrogel coating was fabricated by dissolving the AAO template in 1 M NaOH solution.

Characterization of hydrogel surfaces. The contact angles (CAs) of samples were measured by a Dataphysics OCA20 contact-angle system at room temperature. The average CAs were obtained by measuring three samples in five different positions. The Young's modulus of the hydrogel was measured in the wet state by PeakForce quantitative nanomechanical mapping on an atomic force microscope (AFM, Dimension ICON). We employed a 10 nm tip radius with a setpoint of 1.5 nN. The cantilever movement speed is 5.6 ms, the spring constant is 0.1958 N m^{-1}, and the scan rate is 0.7 Hz.

Preparation of supersaturated CaOx and $CaCO_3$ solutions. According to previous reports, we prepared supersaturated CaOx and $CaCO_3$ solutions. For the supersaturated CaOx solution,[43, 44] a mixture of NaCl (8.8 g, 150 mM), $NaCOOCH_3$ (0.8 g, 5 mM), $CaCl_2$ (0.152 g, 1.4 mM), $Na_2C_2O_4$ (0.132 g, 1 mM) and H_2O (1 l) at pH 7 was stirred for 30 min. For the supersaturated $CaCO_3$ solution,[45] a mixture of $CaCl_2$ (0.111 g, 1 mM) and Na_2HCO_3 (0.168 g, 2 mM) was stirred in 1 l of H_2O.

Adhesion experiments of mineral crystals at room temperature in dynamic and static states. In a dynamic state, nanohair and flat hydrogel coatings (15 mm × 8 mm) were first put into peristaltic pump (Masterflex L/S) pipes with a diameter of 8 mm. Then, 1000 ml of supersaturated CaOx solution was continuously flowed in the pipes at different flow rates (that is, 24, 36, 42, 64, 90, 180, 358 and 717 cm min^{-1}), and after different incubation times (that is, 12, 24, 48 and 96 h), the anti-adhesion performance against mineral crystals on these surfaces was observed by employing an optical microscope (Nikon Ti-E) and a scanning electron microscope (SEM, FEI Quanta 200). In a static state, adhesion experiments were studied only in 500 ml of supersaturated mineral solution (for example, CaOx solution) after different incubation times (that is, 12, 24, 48 and 96 h). Then, the surfaces were taken out and gently washed with deionized water to remove adsorbed mineral solution and non-adhered crystals. Finally, the anti-adhesion performance against mineral crystals on these surfaces was observed by the combination of the optical microscope (Nikon Ti-E) and SEM (FEI Quanta 200).

Dynamic adhesion experiments of mineral crystals at high temperature. First, three kinds of coatings, that is, the nanohair and flat hydrogel coatings and commercial water pipe with a PVC surface, were put into separate peristaltic pump pipes. Then, these coatings were incubated with flowing 80 °C mineral solutions (that is, 1 mM supersaturated CaOx or $CaCO_3$ solutions) for ~24 h. After cooling to room temperature, these coatings were gently taken out from these pump pipes. Following a gentle wash with water, these hydrogel coatings

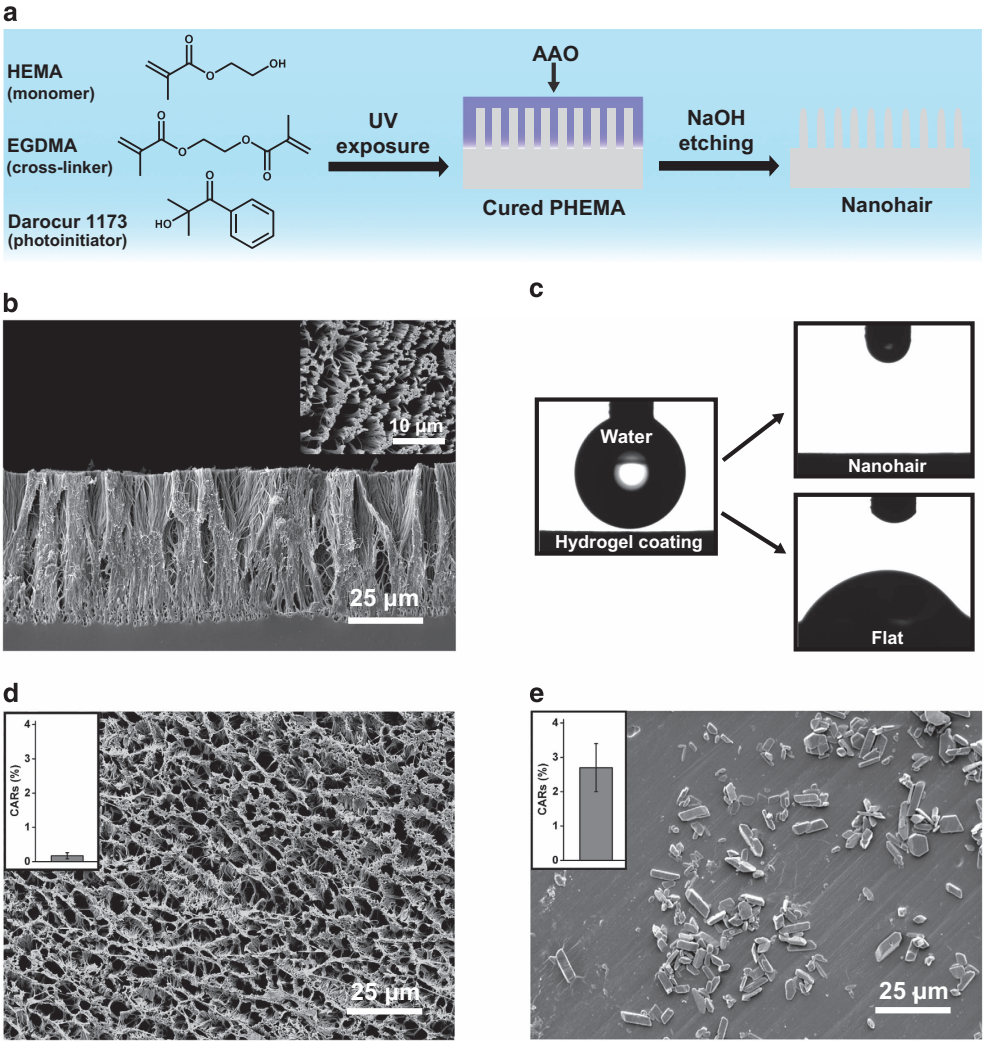

Figure 2 Fabrication and characterization of superhydrophilic nanohair hydrogel coatings. (**a**) Schematic view of the fabrication process of nanohair hydrogel coatings by using the replica molding method. (**b**) Scanning electron microscopic (SEM) images of nanohair hydrogel coatings from a side view and a top view (insert). (**c**) Photographs of water contact angles showing the wettability of the two hydrogel coatings, that is, superhydrophilicity for nanohair hydrogel coatings (top) and hydrophilicity for flat hydrogel coatings (bottom). SEM images of mineral crystal adhesion on (**d**) nanohair and (**e**) flat hydrogel coatings after incubation in a flowing mineral solution (for example, CaOx) for 24 h. The insets show the quantification of mineral crystals adhered on these hydrogel coatings, indicating that the nanohair coatings exhibit highly efficient anti-adhesion against mineral crystals compared to flat coatings. Error bars: standard deviation ($n=3$).

were dried in air for SEM observation and subsequent assessment of mineral adhesion.

RESULTS AND DISCUSSION

We successfully fabricated bio-inspired superhydrophilic hydrogel coatings by integrating photopolymerization with a replica molding method. In brief, a mixture of the monomer HEMA, the cross-linker EGDMA and the photoinitiator Darocur 1173 was illuminated under a mercury lamp through an AAO membrane template. After polymerization, dilute NaOH solution was used to dissolve the AAO templates, forming the PHEMA nanohair hydrogel coatings (Figure 2a). Taking the AAO template with pore size of 200–300 nm as an example, Figure 2b shows the typical nanohair morphology of the as-prepared hydrogel coatings (with a height of 51.0 ± 3.8 μm and a diameter of ca. 400 nm). As shown in Figure 2c, the nanohair hydrogel coating is superhydrophilic with a CA of approximately 0°. In comparison, the flat hydrogel coating is hydrophilic with a CA of 58 ± 4°. Therefore, we successfully obtained a superhydrophilic hydrogel coating with nanohair surface morphology.

Then, we compared the anti-adhesion performance against mineral crystals on the nanohair and flat hydrogel coatings under flow conditions. The SEM images presented in Figures 2d and e show that there are many crystals aggregated on the flat hydrogel coatings but few on the nanohair ones (with a height of 51.0 ± 3.8 μm) upon exposure to a flowing mineral solution (that is, CaOx). In addition, as shown in Supplementary Figure S1, energy dispersive X-ray spectroscopy (EDS) analysis was employed to further verify the distribution of CaOx crystals on hydrogel coatings in a dynamic state. The calcium signals show that abundant mineral crystals adhered onto the flat hydrogel coatings, whereas few crystals adhered on top of the nanohair hydrogel coatings. Moreover, the mineral crystals were not observed among the interspaces of these nanohairs, as indicated by the SEM images and corresponding EDS analysis of the cross-section of the nanohair hydrogel. Supplementary Figure S2a shows that most of the

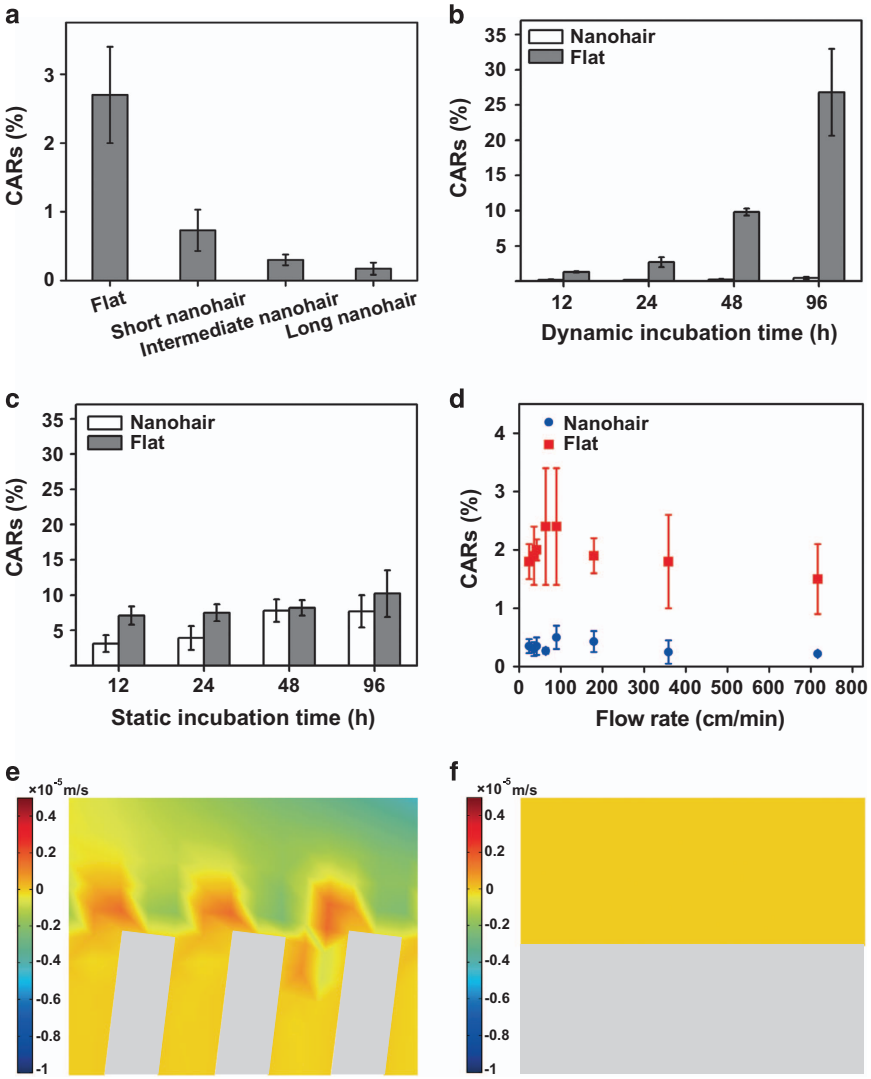

Figure 3 Influence of nanohair length, incubation time and flow rate on the adhesion of mineral crystals. (**a**) In a dynamic state, the crystal adhesion ratios (CARs) significantly reduced with increasing nanohair lengths. (**b**) With the incubation time increasing from 12 to 96 h, the amount of crystals adhered onto the flat hydrogel coatings is always greater than that on the nanohair hydrogel coatings (51.0 ± 3.8 μm) in a dynamic state (that is, a flow rate of 24 cm min^{-1}), revealing the excellent anti-adhesion property of nanohair hydrogel coatings. (**c**) In a static state, before 48 h of incubation, the crystals adhered on nanohair the hydrogel coatings are slightly less than those on flat hydrogel coatings. After 48 h of incubation, the amount of crystals adhered onto both coatings is similar, suggesting that nanohair hydrogel coatings nearly lose their efficient anti-adhesion property in a static state. (**d**) With mineral solution at flow rates varying from 24 to 717 cm min^{-1}, the nanohair hydrogel coatings always display a more efficient anti-adhesion property than the flat ones, even at a low flow rate (that is, 24 cm min^{-1}). The numerical simulation shows the distributions of velocity in the y direction on (**e**) nanohair and (**f**) flat surfaces. Error bars: standard deviation ($n = 3$).

mineral crystals adhered to the top surface of the nanohair hydrogel coatings and that hardly any crystals were embedded in the gap region of the nanohairs, which is in accordance with the corresponding EDS results (Supplementary Figure S2b and c). There was a high calcium content on the top surface of the nanohair hydrogel (Supplementary Figure S2b) but a lower intensity of calcium in the gap region of the nanohair hydrogel (Supplementary Figure S2c). Therefore, mineral crystals adhered only onto the top surface of the hydrogel coatings. To quantitatively estimate the anti-adhesion performance against mineral crystals on these coatings, we determined the crystal adhesion ratios (CARs) by calculating the value of $S_{crystal}/S_{total}$ ($S_{crystal}$ = crystal coverage area, and S_{total} = total surface area) from their corresponding SEM images through ImageJ software.[46] Compared with the flat hydrogel coatings, he nanohair ones exhibited up to a 93% reduction in CAR after 24 h of incubation (inset in Figures 2d and e). Therefore, these results reveal that the introduction of nanohair morphology endows the hydrogel coatings with high anti-adhesion against mineral crystals under flow conditions.

We further characterized the wettability and anti-adhesion properties of nanohair hydrogel coatings with different lengths. First, by employing AAO templates with depths ranging from 2 to 60 μm, we obtained three kinds of nanohair hydrogel coatings with different lengths: 0.4 ± 0.1 μm for short nanohairs, 21.5 ± 3.0 μm for intermediate nanohairs and 51.0 ± 3.8 μm for long nanohairs (Supplementary Figure S3). Then, the wettability was determined by monitoring the CAs of these nanohair coatings. As shown in Figure 2c and Supplementary Figure S4, the CAs gradually decrease following the increase in the nanohair lengths. When the length is >20 μm, the

CAs of the nanohair surfaces all decrease to ~0°. These results indicate the nanohair morphology can improve the hydrophilicity of the as-prepared hydrogel coatings, which is consistent with the basic principle of the Wenzel theory.[47] Next, experiments evaluating anti-adhesion against mineral crystals were performed on the above-mentioned hydrogel coatings, and the flat coating was chosen as the control. As shown in Figure 3a, the CARs of the nanohair hydrogel coatings clearly reduced as the nanohair length gradually increased. Compared with the flat hydrogel coatings (CARs of $2.70 \pm 0.70\%$), the nanohair hydrogel coatings exhibit considerable anti-adhesion performance against mineral crystals (CARs of $0.73 \pm 0.30\%$ for the short nanohairs), especially for the superhydrophilic intermediate and long nanohairs (CARs of $0.30 \pm 0.08\%$ and $0.17 \pm 0.09\%$, respectively), which may be because water molecules preferentially approach the superhydrophilic surface of PHEMA nanohairs, thereby reducing the growth of mineral crystals,[48] and because the abundant -OH groups also promote resistance against the adhesion of these mineral crystals.[49] Therefore, the superhydrophilic property and surface structure of the nanohair hydrogel coatings probably contribute to their unique anti-scaling property.

To further characterize this anti-adhesion behavior, we performed adhesion experiments with CaOx crystals on two kinds of hydrogel coatings (that is, nanohair and flat) with different incubation times and flow rates. In a dynamic state, the amount of adhered crystals on the flat hydrogel coatings rapidly increased from $1.3 \pm 0.1\%$ to $26.8 \pm 6.2\%$ as the incubation time was prolonged from 12 to 96 h, respectively (Figure 3b and Supplementary Figure S5a). In comparison, the nanohair hydrogel coatings (long nanohairs with a height of 51.0 ± 3.8 μm) always maintain a high anti-adhesion capability with negligible CARs (0.5%). However, in a static state, the CARs on the two kinds of hydrogel coatings gradually became closer to each other with increasing incubation time (Figure 3c and Supplementary Figure S5b). The significant reduction in the amount of mineral crystals adhered onto the nanohair hydrogel coatings is probably due to the fluid-assisted passive motion of the nanohairs,[50,51] which can repel crystals away from the surfaces and further prevent the aggregation of crystals. In addition, we systematically explored the influence of flow rates on CaOx crystal adhesion. With the flow rates varied from 24 to 717 cm min^{-1}, nanohair hydrogel coatings always displayed high anti-adhesion properties with $<0.5\%$ CARs, even at a lower flow rate (that is, 24 cm min^{-1}; Figure 3d). By contrast, a

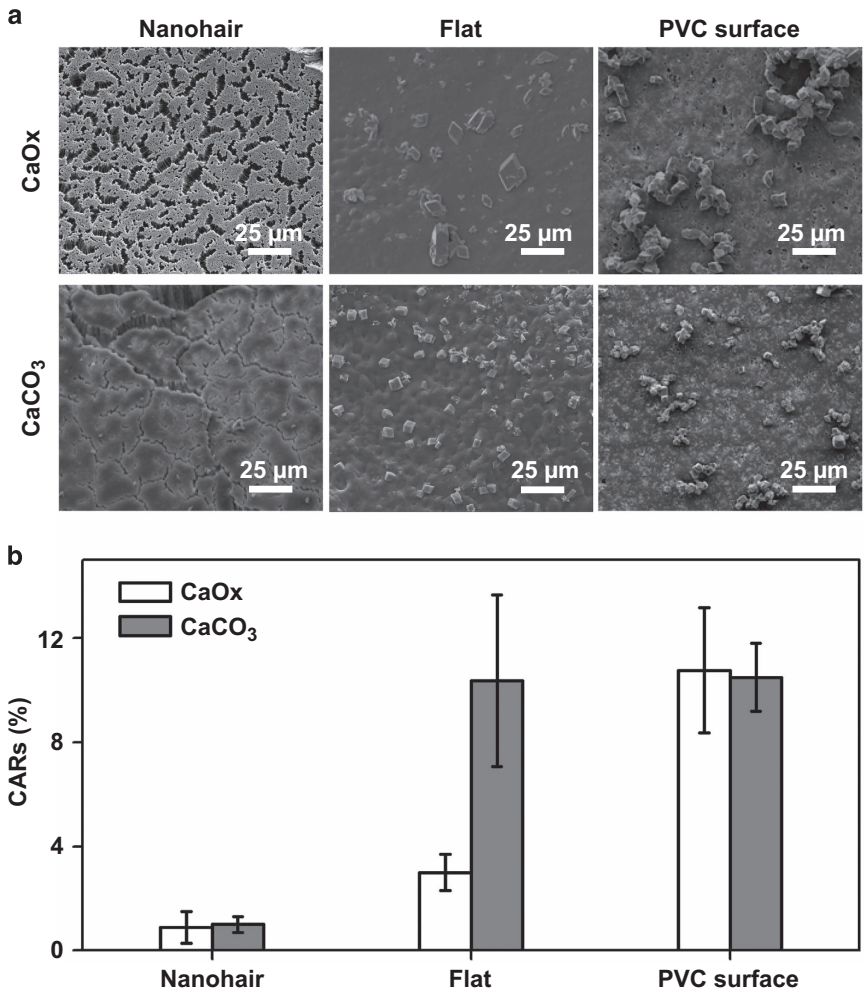

Figure 4 Comparison of anti-adhesion performance against mineral crystals on nanohair and flat hydrogel coatings with that on a commercial water pipe with a polyvinylchloride (PVC) surface at a high temperature of 80 °C. (**a**) After incubation in a flowing mineral solution (for example, CaOx or $CaCO_3$ solution) for 24 h, the nanohair hydrogel coatings show barely any adhered mineral crystal in their SEM images compared with the flat coatings and PVC surfaces. (**b**) Quantitative analysis reveals that the nanohair hydrogel coatings possess better anti-scaling capability than the other two coatings. Error bars: standard deviation ($n = 3$).

greater than 4-fold increase in crystal adhesion can be observed on the flat coatings at the same flow rate. Furthermore, the nanohair hydrogel coatings retain their surface morphologies after exposure to a high flow rate of 717 cm min^{-1}, as shown in Supplementary Figure S6, suggesting their structural stability under high flow conditions. Therefore, flow conditions are necessary to realize the high anti-adhesion performance on nanohair hydrogel coatings.

We have carried out preliminary numerical simulations to understand the underlying physics of the anti-adhesive property of the PHEMA nanohairs. We compared fluid-structure interactions using COMSOL software. The detailed setup can be shown in the Supplementary Information and Supplementary Figure S7. Velocity magnitudes on the nanohair and flat surfaces were compared in Supplementary Figure S8, showing that the velocity distribution is laminar except around the tops of the nanohair and flat surfaces. Moreover, we also observed a ratchet-like distribution of velocity in the y direction for the nanohair surface (Figure 3e), while the velocity in the y direction was zero for the flat surface (Figure 3f). The ratchet-like velocity distribution may be due to the uneven distribution of the flow-induced force acting on the crystal surface, thereby providing the anti-scaling capability of the nanohair surface.

However, in practical applications (for example, high temperatures), most scale inhibitors (for example, traditional chelating agents and naturally occurring polymers) are greatly limited because they are unstable; thus, a higher inhibitor concentration is required,[52] which can even cause environmental pollution[53]. Therefore, we further compared the anti-adhesion performance against mineral crystals on the nanohair and flat hydrogel coatings with that on a commercial water pipe with a PVC surface in a hot flowing mineral solution (for example, 1 mM CaOx or $CaCO_3$ solution at a temperature of 80 °C). As depicted in Figure 4a, the nanohair hydrogel coatings (with a height of 51.0 ± 3.8 μm) showed lower adhesion of both CaOx and $CaCO_3$ crystals than the flat coatings and PVC surfaces after 24 h of incubation. Figure 4b shows the evaluation of the anti-adhesion properties against mineral scales of these coatings, which can be further verified by the distribution of chemical components such as calcium in the EDS data analysis presented in Supplementary Figure S9. The CARs of crystals (for example, $CaCO_3$) on the nanohair hydrogel coatings are $0.9 \pm 0.6\%$, which is nearly 11-fold lower than those on the flat hydrogel coatings ($10.4 \pm 3.3\%$) and PVC surfaces ($10.5 \pm 1.3\%$). In addition, before and after immersion in the hot mineral solutions, the nanohair hydrogel coatings exhibit a similar average Young's modulus (3.99 and 3.80 MPa) and structural features (Supplementary Figure S6), suggesting their excellent mechanical stability. Therefore, these results indicate that nanohair hydrogel coatings can maintain their stable anti-adhesion property at high temperature.

CONCLUSION

In summary, we demonstrate the fabrication of bio-inspired superhydrophilic nanohair hydrogel coatings and their excellent anti-adhesion property against mineral crystals under dynamic fluid flow. The high anti-adhesion property can probably be attributed to the superhydrophilicity and fluid-assisted motion of the nanohair structure, which inhibit the adhesion of mineral crystals onto the surface. Furthermore, nanohair hydrogel coatings retain their strong anti-adhesion capability at high temperature. This study provides a novel bio-inspired strategy for designing high anti-scaling coatings for water supply and drainage systems.

CONFLICT OF INTEREST

The authors declare no conflict of interest.

ACKNOWLEDGEMENTS

This research is supported by the National Natural Science Foundation of China (21501184, 21425314, 21434009 and 21421061), MOST (2013YQ190467), the Top-Notch Young Talents Program of China, and the Youth Innovation Promotion Association, CAS (2017036).

PUBLISHER'S NOTE

1 Meyers, M. A., Chen, P. Y., Lin, A. Y. M. & Seki, Y. Biological materials: structure and mechanical properties. *Prog. Mater. Sci.* **53**, 1–206 (2008).
2 Labonte, D. & Federle, W. Scaling and biomechanics of surface attachment in climbing animals. *Philos. Trans. R. Soc. B* **370**, 20140027 (2015).
3 Gu, Z., Li, S., Zhang, F. & Wang, S. Understanding surface adhesion in nature: a peeling model. *Adv. Sci.* **3**, 1500327 (2016).
4 Autumn, K., Liang, Y. A., Hsieh, S. T., Zesch, W., Chan, W. P., Kenny, T. W., Fearing, R. & Full, R. J. Adhesive force of a single gecko foot-hair. *Nature* **405**, 681–685 (2005).
5 Stark, A. Y., Badge, I., Wucinich, N. A., Sullivan, T. W., Niewiarowski, P. H. & Dhinojwala, A. Surface wettability plays a significant role in gecko adhesion underwater. *Proc. Natl Acad. Sci. USA* **110**, 6340–6345 (2013).
6 Geim, A. K., Dubonos, S. V., Grigorieva, I. V., Novoselov, K. S., Zhukov, A. A. & Shapoval, S. Y. Microfabricated adhesive mimicking gecko foot-hair. *Nat. Mater.* **2**, 461–463 (2003).
7 Lee, H., Dellatore, S. M., Miller, W. M. & Messersmith, P. B. Mussel-inspired surface chemistry for multifunctional coatings. *Science* **318**, 426–430 (2007).
8 Zhao, Q., Lee, D. W., Ahn, B. K., Seo, S., Kaufman, Y., Israelachvili, J. N. & Waite, J. H. Underwater contact adhesion and microarchitecture in polyelectrolyte complexes actuated by solvent exchange. *Nat. Mater.* **15**, 407–412 (2016).
9 Lee, H., Lee, B. P. & Messersmith, P. B. A reversible wet/dry adhesive inspired by mussels and geckos. *Nature* **448**, 338–341 (2007).
10 Lu, Y., Aimetti, A. A., Langer, R. & Gu, Z. Bioresponsive materials. *Nat. Rev. Mater* **1**, 16075 (2016).
11 Kwak, M. K., Jeong, H. E. & Suh, K. Y. Rational design and enhanced biocompatibility of a dry adhesive medical skin patch. *Adv. Mater.* **23**, 3949–3953 (2011).
12 Gao, W., Emaminejad, S., Nyein, H. Y. Y., Challa, S., Chen, K., Peck, A., Fahad, H. M., Shiraki, H., Ota, H., Kiriya, D., Lien, D. H., Brooks, G. A., Davis, R. W. & Javey, A. Fully integrated wearable sensor arrays for multiplexed in situ perspiration analysis. *Nature* **529**, 509–514 (2016).
13 Lee, H., Choi, T. K., Lee, Y. B., Cho, H. R., Ghaffari, R., Wang, L., Choi, H. J., Chung, T. D., Lu, N., Hyeon, T., Choi, S. H. & Kim, D. H. A graphene-based electrochemical device with thermoresponsive microneedles for diabetes monitoring and therapy. *Nat. Nano* **11**, 566–572 (2016).
14 Koh, A., Kang, D., Xue, Y., Lee, S., Pielak, R. M., Kim, J., Hwang, T., Min, S., Banks, A., Bastien, P., Manco, M. C., Wang, L., Ammann, K. R., Jang, K. I., Won, P., Han, S., Ghaffari, R., Paik, U., Slepian, M. J., Balooch, G., Huang, Y. & Rogers, J. A. A soft, wearable microfluidic device for the capture, storage, and colorimetric sensing of sweat. *Sci. Transl. Med* **8**, 366ra165 (2016).
15 Imani, S., Bandodkar, A. J., Mohan, A. M. V., Kumar, R., Yu, S., Wang, J. & Mercier, P. P. A wearable chemical-electrophysiological hybrid biosensing system for real-time health and fitness monitoring. *Nat. Commun.* **7**, 11650 (2016).
16 Ryu, J., Hee, Ku, S., Lee, H. & Beum Park, C. Mussel-inspired polydopamine coating as a universal route to hydroxyapatite crystallization. *Adv. Funct. Mater.* **20**, 2132–2139 (2010).
17 Antony, A., Low, J. H., Gray, S., Childress, A. E., Le-Clech, P. & Leslie, G. Scale formation and control in high pressure membrane water treatment systems: a review. *J. Membr. Sci.* **383**, 1–16 (2011).
18 Walker, P. & Sheikholeslami, R. Assessment of the effect of velocity and residence time in $CaSO_4$ precipitating flow reaction. *Chem. Eng. Sci.* **58**, 3807–3816 (2003).
19 Alabi, A., Chiesa, M., Garlisi, C. & Palmisano, G. Advances in anti-scale magnetic water treatment. *Environ. Sci. Water Res. Technol.* **1**, 408–425 (2015).
20 Popov, K. I., Kovaleva, N. E., Rudakova, G. Y., Kombarova, S. P. & Larchenko, V. E. Recent state-of-the-art of biodegradable scale inhibitors for cooling-water treatment applications. *Therm. Eng* **63**, 122–129 (2016).
21 Tijing, L. D., Yu, M.-H., Kim, C. H., Amarjargal, A., Lee, Y. C., Lee, D. H., Kim, D. W. & Kim, C. S. Mitigation of scaling in heat exchangers by physical water treatment using zinc and tourmaline. *Appl. Therm. Eng.* **31**, 2025–2031 (2011).
22 Nishida, I. Precipitation of calcium carbonate by ultrasonic irradiation. *Ultrason. Sonochem.* **11**, 423–428 (2004).
23 Liu, L., Yang, L. Q., Liang, H. W., Cong, H. P., Jiang, J. S. & Yu, H. Bio-inspired fabrication of hierarchical FeOOH nanostructure array films at the air-water interface,

their hydrophobicity and application for water treatment. *ACS Nano* **7**, 1368–1378 (2013).
24 Bu, Y., Zhou, Y., Yao, Q., Chen, Y., Sun, W. & Wu, W. Preparation and evaluation of nonphosphate terpolymer as scale inhibitor and dispersant for $Ca_3(PO_4)_2$, $BaSO_4$, and Iron (III) hydroxide scales. *J. Appl. Polym. Sci.* **132**, 41546–41556 (2014).
25 Chu, Z., Feng, Y. & Seeger, S. Oil/water separation with selective superantiwetting/superwetting surface materials. *Angew. Chem. Int. Ed.* **54**, 2328–2338 (2015).
26 Wang, S., Liu, K., Yao, X. & Jiang, L. Bioinspired surfaces with superwettability: new insight on theory, design, and applications. *Chem. Rev.* **115**, 8230–8293 (2015).
27 Hou, X., Hu, Y., Grinthal, A., Khan, M. & Aizenberg, J. Liquid-based gating mechanism with tunable multiphase selectivity and antifouling behaviour. *Nature* **519**, 70–73 (2015).
28 Tian, X., Jokinen, V., Li, J., Sainio, J. & Ras, R. H. Unusual Dual Superlyophobic Surfaces in Oil-Water Systems: The Design Principles. *Adv. Mater.* **28**, 10652–10658 (2016).
29 Jiang, W., He, J., Xiao, F., Yuan, S., Lu, H. & Liang, B. Preparation and antiscaling application of superhydrophobic anodized CuO nanowire surfaces. *Ind. Eng. Chem. Res.* **54**, 6874–6883 (2015).
30 Li, H., Yu, S., Han, X. & Zhao, Y. A stable hierarchical superhydrophobic coating on pipeline steel surface with self-cleaning, anticorrosion, and anti-scaling properties. *Colloids Surf. A* **503**, 43–52 (2016).
31 Cheong, W. C., Gaskell, P. H. & Neville, A. Substrate effect on surface adhesion/crystallisation of calcium carbonate. *J. Cryst. Growth* **363**, 7–21 (2013).
32 Tsujihata, M. Mechanism of calcium oxalate renal stone formation and renal tubular cell injury. *Int. J. Urol.* **15**, 115–120 (2008).
33 Vervaet, B. A., Verhulst, A., Broe, M. E., De & D'Haese, P. C. The tubular epithelium in the initiation and course of intratubular nephrocalcinosis. *Urol. Res.* **38**, 249–256 (2010).
34 Pfaller, W., Cstraunthaler, G. & Loidl, P. Morphology of the differentiation and maturation of LLC-PK1 epithelia. *J. Cell. Physiol.* **142**, 247–254 (1990).
35 Crawley, S. W., Mooseker, M. S. & Tyska, M. J. Shaping the intestinal brush border. *J. Cell Biol.* **207**, 441–451 (2014).
36 Verkoelen, C. F. & Verhulst, A. Proposed mechanisms in renal tubular crystal retention. *Kidney Int.* **72**, 13–18 (2007).
37 Bergeron, M., Thiéry, G., Lenoir, F., Giocondi, M. C. & Legrimellec, C. Organization of the endoplasmic reticulum in renal cell lines MDCK and LLC-PK1. *Cell Tissue Res.* **277**, 297–307 (1994).
38 Rabinovich, Y. I., Esayanur, M., Daosukho, S., Byer, K. J., El-Shall, H. E. & Khan, S. R. Adhesion force between calcium oxalate monohydrate crystal and kidney epithelial cells and possible relevance for kidney stone formation. *J. Colloid Interface Sci.* **300**, 131–140 (2006).
39 Rebelo, L., Carmo-Fonseca, M. & Moura, T. F. Redistribution of microvilli and membrane enzymes in isolated rat proximal tubule cells. *Biophys. J.* **74**, 203–209 (1992).
40 Mager, M. D., LaPointe, V. & Stevens, M. M. Exploring and exploiting chemistry at the cell surface. *Nat. Chem.* **3**, 582–589 (2011).
41 Kenny, A. J. & Maroux, S. Topology of microvillar membrance hydrolases of kidney and intestine. *Physiol. Rev.* **62**, 91–128 (1982).
42 Chandra, D., Taylor, J. A. & Yang, S. Replica molding of high-aspect-ratio (sub-) micron hydrogel pillar arrays and their stability in air and solvents. *Soft Matter* **4**, 979–984 (2008).
43 Taller, A., Grohe, B., Rogers, K. A., Goldberg, H. A. & Hunter, G. K. Specific adsorption of osteopontin and synthetic polypeptides to calcium oxalate monohydrate crystals. *Biophys. J.* **93**, 1768–1777 (2007).
44 Liu, Y., Mao, H. Y., Liu, X. F., Qiao, L. J. & Guo, R. Calcium oxalate crystallization in the presence of amphiphilic phosphoproteins. *CrystEngComm* **16**, 8841–8851 (2014).
45 Shen, Z. H., Li, J. S., Xu, K., Ding, L. L. & Ren, H. Q. The effect of synthesized hydrolyzed polymaleic anhydride (HPMA) on the crystal of calcium carbonate. *Desalination* **284**, 238–244 (2012).
46 Anh, T. T. H., Xing, M., Le, T., Huynh, D., Sugawara-Narutaki, A. & Fong, E. Elastin-based silver-binding proteins with antibacterial capabilities. *Nanomedicine* **8**, 567–575 (2013).
47 Wenzel, R. N. Resistance of solid surfaces to wetting by water. *Ind. Eng. Chem.* **28**, 988–994 (1936).
48 Yamanaka, S., Ito, N., Shimosaka, A., Shirakawa, Y. & Hidaka, J. AFM investigation for the initial growth processes of calcium carbonate on hydrophilic and hydrophobic substrate. *Cryst. Growth Des.* **9**, 3245–3250 (2009).
49 Sheng, X. X., Jung, T. S., Wesson, J. A. & Ward, M. D. Adhesion at calcium oxalate crystal surfaces and the effect of urinary constituents. *Proc. Natl Acad. Sci. USA* **102**, 267–272 (2005).
50 Bhattacharya, A. & Balazs, A. C. Stiffness-modulated motion of soft microscopic particles over active adhesive cilia. *Soft Matter* **9**, 3945–3955 (2013).
51 Tripathi, A., Shum, H. & Balazs, A. C. Fluid-driven motion of passive cilia enables the layer to expel sticky particles. *Soft Matter* **10**, 1416–1427 (2014).
52 Li, G., Guo, S., Zhang, J. & Liu, Y. Inhibition of scale buildup during produced-water reuse: Optimization of inhibitors and application in the field. *Desalination* **351**, 213–219 (2014).
53 Xu, Y., Zhao, L., Wang, L., Xu, S. & Cui, Y. Synthesis of polyaspartic acid-melamine grafted copolymer and evaluation of its scale inhibition performance and dispersion capacity for ferric oxide. *Desalination* **286**, 285–289 (2012).

Supplementary Information accompanies the paper on the NPG Asia Materials website (http://www.nature.com/am)